Volume 47
Number 6
14 February 2023
Pages 2685–3186

NJC

New Journal of Chemistry

A journal for new directions in chemistry

rsc.li/njc

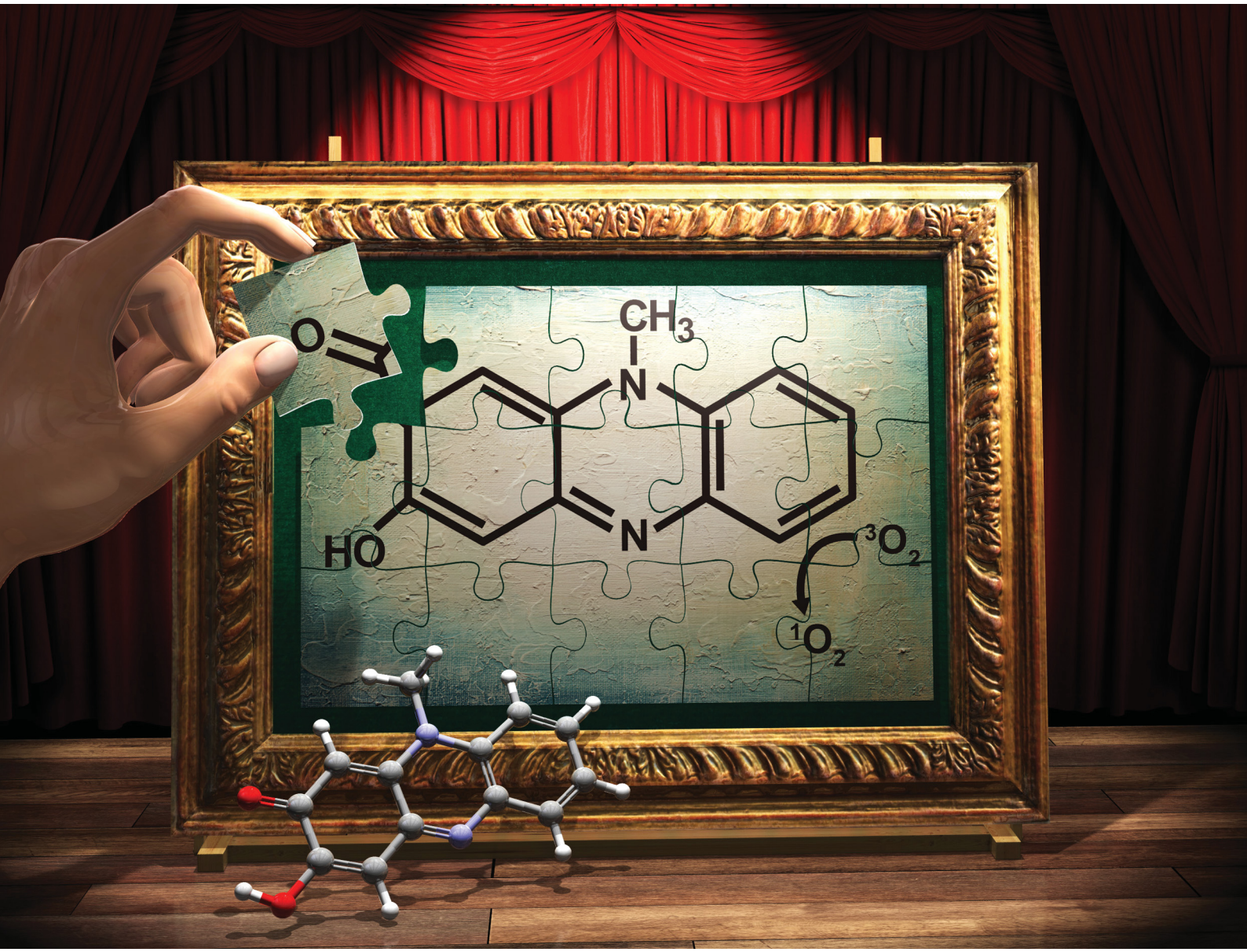

ISSN 1144-0546

ROYAL SOCIETY OF CHEMISTRY

PAPER

Yousuke Ooyama *et al.*

Synthesis and optical properties of phenazinone-based photosensitizers for singlet oxygen generation

cnrs

NJC

ROYAL SOCIETY OF CHEMISTRY

PAPER

Cite this: *New J. Chem.*, 2023, **47**, 2711

Synthesis and optical properties of phenazinone-based photosensitizers for singlet oxygen generation†

Kazuki Ohira, Masahiro Yamamoto, Keiichi Imato and Yousuke Ooyama *

Phenazinone derivatives **PZ1–3** where a carbonyl group is incorporated into the chromophore are designed and developed as halogen-atom-free-heteroanthracene-based photosensitizers possessing the ability to generate singlet oxygen ($^1O_2$). Compared to the phenazine-2,3-diol (**PZ**) without a carbonyl group, the molar absorption coefficients of **PZ1–3** at around 480 nm increased by a factor of five to six. Furthermore, the values of fluorescence quantum yields (Φ_{fl}) of **PZ1–3** were significantly low (0.03 for **PZ1**, 0.04 for **PZ2**, and 0.05 for **PZ3**). To evaluate the $^1O_2$ generation ability of **PZ1–3**, the $^1O_2$ quantum yields (Φ_Δ) of **PZ1–3** were estimated and it was demonstrated that **PZ1** exhibited a higher Φ_Δ value than rose bengal (RB) known as a reference photosensitizer to generate $^1O_2$ (0.86 for **PZ1**, 0.54 for **PZ2**, 0.069 for **PZ3**, and 0.68 for RB). Moreover, the rate constants (k_r, k_{nr}, k_{ISC}, and k_{IC}) of **PZ1–3** indicated that the reason for the low Φ_Δ of **PZ2** and **PZ3** comes from the vibrational relaxation caused by a flexible methoxymethoxy and 4-chlorobenzoate group, respectively. Density functional theory (DFT), time-dependent DFT (TD-DFT), and natural transition orbital (NTO) calculations suggested that for **PZ1–3**, the intersystem crossing (ISC) processes from the lowest excited singlet state (S_1) to the third triplet state (T_3) are thermodynamically feasible and facilitated based on El-Sayed's rule. Consequently, we propose that the phenazinone skeleton is one of the promising halogen-atom-free-heteroanthracene-based chromophore photosensitizers.

Received 31st October 2022,
Accepted 17th December 2022

DOI: 10.1039/d2nj05322e

rsc.li/njc

Introduction

Photosensitizers (PSs) possessing the singlet oxygen ($^1O_2$) generation ability have attracted much attention because of their useful applications such as in water purification,[1] antivirals,[2] and photodynamic therapy (PDT) for cancer treatment.[3] These PSs generally produce $^1O_2$ through the following processes: initially, the photosensitizer (S_0) absorbs light ($h\nu$) to generate the singlet excited state of the photosensitizer (S_n), and then the photoexcited sensitizer (S_n) undergoes intersystem crossing (ISC) to generate the triplet excited state (T_n). After internal conversion (IC) to the lowest excited triplet state (T_1), subsequent energy transfer from the photoexcited PS (T_1) to triplet oxygen ($^3O_2$) produces $^1O_2$.[4] Indeed, phthalocyanine dyes,[5] phenothiazine dyes,[6] xanthene dyes,[7] and boron-dipyrromethene (BODIPY) dyes[8] are known to show high $^1O_2$ quantum yield (Φ_Δ) values. For these PSs, halogen atoms such as iodide and bromide atoms are often introduced into the chromophores to promote ISC based on spin–orbit coupling,[9] but it raises concerns about dark cytotoxicity.[10] To overcome the drawbacks, halogen-atom-free PSs[11] such as a family of heteroanthracenes have been extensively studied. Among them, methylene blue (MB) is used as a reference PS for the evaluation of Φ_Δ.[12] Therefore, in order to create a new type of halogen-atom-free-heteroanthracene-based PS, we have focused on the phenazine skeleton, because to the best of our knowledge there are few reports on the evaluation of $^1O_2$ generation ability for phenazine derivatives.[13] In our previous study,[14] we have developed phenazine-2,3-diol-based PSs (**KO-0–3**) and demonstrated that the modification of the phenazine-2,3-diol chromophore with formyl groups promotes ISC, leading to efficient $^1O_2$ generation (Fig. 1a). According to the El-Sayed rule,[15] formyl and carbonyl substituents in a chromophore skeleton allow ISC by a change in the molecular orbital type, such as $^1(n\pi^*)$ to $^3(\pi\pi^*)$ and $^1(\pi\pi^*)$ to $^3(n\pi^*)$ transitions. Indeed, these PSs exhibited moderate photosensitizing properties for $^1O_2$ generation (Φ_Δ = 0.41 for **KO-3**).

Recently, in our continuous work to develop halogen-atom-free PSs based on El-Sayed's rule, it was found that 3-hydroxy-10-methylphenazin-2(10*H*)-one (**PZ1**) incorporating a carbonyl

Applied Chemistry Program, Graduate School of Advanced Science and Engineering, Hiroshima University, 1-4-1 Kagamiyama, Higashi-Hiroshima, 739-8527, Japan. E-mail: yooyama@hiroshima-u.ac.jp

† Electronic supplementary information (ESI) available. CCDC 2194829, 2194831 and 2194832. For ESI and crystallographic data in CIF or other electronic format see DOI: https://doi.org/10.1039/d2nj05322e

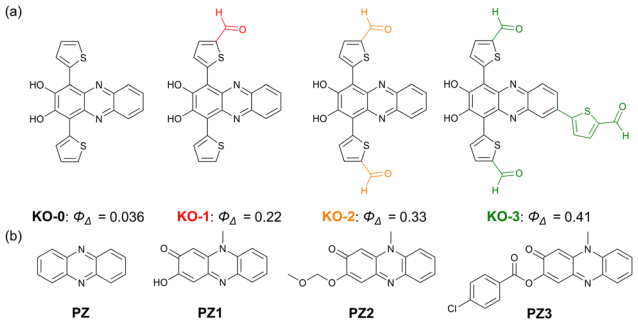

Fig. 1 (a) Chemical structures of phenazine-2,3-diol-based PSs **KO-0–3** and their Φ_Δ values employed in our previous study. (b) Chemical structures of phenazine-2,3-diol (**PZ**) and phenazinone-based PSs **PZ1–3** designed and synthesized in this study.

group into the chromophore possesses highly efficient photosensitizing capabilities compared to phenazine-2,3-diol-based PSs (Fig. 1b). Indeed, **PZ1** without halogen atoms possesses the superior $^1O_2$ generation ability to RB (Φ_Δ = 0.68 in THF) with many halogen atoms as well as MB (Φ_Δ = 0.57 in dichloromethane)[21] without halogen atoms. Based on our previous study and El-Sayed's rule, it was assumed that the carbonyl moiety in **PZ1** plays an essential role in the efficient ISC, that is, high Φ_Δ value. In order to confirm the presence of a carbonyl group in **PZ1**, X-ray single crystal structure analyses were required. Therefore, we have designed and synthesized the phenazinone derivative **PZ3** with a 4-chlorobenzoate group. It is well known that the 4-chlorobenzoate group is able to improve crystallizability.[16] Fortunately, we succeeded in performing X-ray single crystal structure analyses for **PZ1** as well as **PZ3**. Furthermore, it was found that the Φ_Δ values are significantly different between **PZ1** and **PZ3**. Therefore, in order to investigate the substituent effects on the optical and $^1O_2$ generation properties between the phenazinone-based PSs, we prepared **PZ2** with a methoxymethoxy group as a substitute for the hydroxy group. Moreover, the density functional theory (DFT), time-dependent DFT (TDDFT), and natural transition orbital (NTO) calculations were performed to evaluate the ISC efficiency of phenazinone-based PSs. Herein, we report the phenazinone chromophore as a new family of heteroanthracene-based PSs without halogen atoms for efficient $^1O_2$ generation.

Results and discussion

Synthesis

PZ1 was prepared in one step by the cyclodehydration of *N*-methyl-*o*-phenylenediamine and 2,5-dihydroxy-1,4-benzoquinone (Scheme 1). In order to perform X-ray single crystal structure analyses, we designed phenazinone derivative **PZ3** with a 4-chlorobenzoate group which is able to improve crystallizability.[16] In addition, in order to investigate the substituent effects on the optical and $^1O_2$ generation properties, we devised **PZ2** with a methoxymethoxy group as a substitute for the hydroxy group. The reactions of **PZ1** with chloromethyl

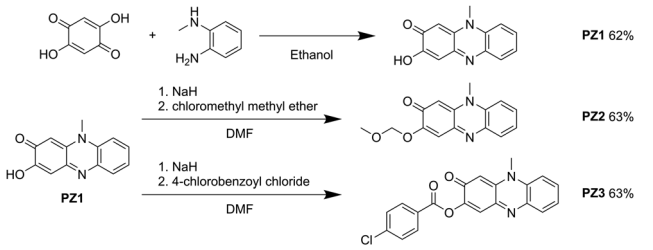

Scheme 1 Synthetic routes of **PZ1–3**.

methyl ether or 4-chlorobenzoyl chloride gave **PZ2** and **PZ3**, respectively. These PSs were obtained in moderate yields (62–63%) and successfully characterized by ^{1}H NMR, ^{13}C NMR, FTIR, and high-resolution mass spectrometric analysis. Furthermore, X-ray single crystal analysis was performed on the PSs.

X-Ray crystal structures

As shown in Fig. 2, for all the three PSs, the bond lengths of C2–O1 and C3–O2 are *ca.* 1.25 Å and *ca.* 1.36 Å, respectively. Therefore, C2–O1 and C3–O2 have typical C=O double bond and C–O single bond lengths, respectively, indicating undoubtedly that the three PSs have a phenazinone skeleton. Interestingly, **PZ1**, **PZ2**, and **PZ3** have high planarity with small root-mean-square deviations of 0.0487, 0.0717, and 0.1033 Å, respectively, despite the presence of an sp^3 nitrogen atom.

Optical properties

The photoabsorption and fluorescence spectra of **PZ1–3** in THF are shown in Fig. 3 with comparison to those of phenazine-2,3-diol (**PZ**), and their optical data are summarized in Table 1. **PZ** showed two photoabsorption maximums (λ_{max}^{abs}): a narrow band at around 390 nm is attributed to the $\pi \rightarrow \pi^*$ transition of the phenazine skeleton which is supported by DFT calculations (Table S6 and Fig. S16, ESI†), and the other weak band at around 480 nm (molar extinction coefficient (ε) = 1700 M^{-1} cm^{-1}) is ascribable to the formation of phenoxide ions by the partial deprotonation of the hydroxyl groups.[13] On the other hand, **PZ1** exhibited an intense photoabsorption band with a λ_{max}^{abs} (ε = 10 900 M^{-1} cm^{-1}) at 478 nm[17] compared to **PZ**. It was found that the introduction of the methoxymethoxy group or 4-chlorobenzoate group into the phenazinone chromophore

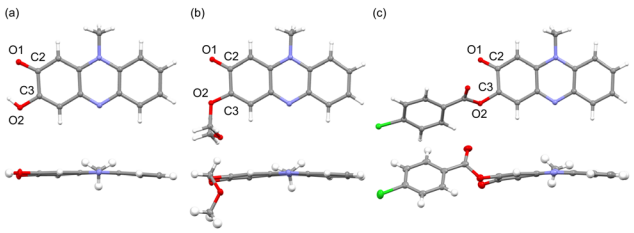

Fig. 2 X-Ray crystal structures of (a) **PZ1**, (b) **PZ2**, and (c) **PZ3**. Selected bond lengths (Å): C2–O1 1.2566(18), 1.2418(16), and 1.2422(15), C3–O2 1.3436(18), 1.3582(15), and 1.3906(15) for **PZ1**, **PZ2**, and **PZ3**, respectively.

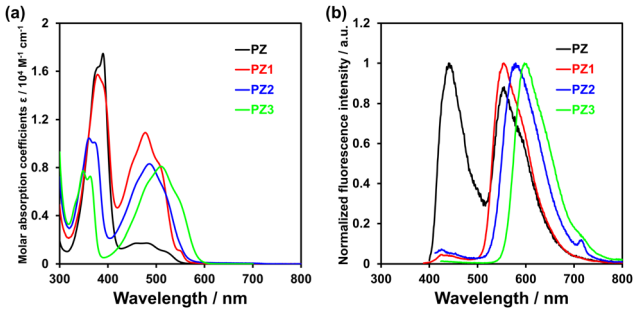

Fig. 3 (a) Photoabsorption and (b) fluorescence (λ_{ex} = 361–390 nm) spectra of **PZ** and **PZ1–3** (1.0×10^{-4} M) in THF.

leads to a further bathochromic shift of the photoabsorption band (λ_{max}^{abs} = 487 nm for **PZ2** and 510 nm for **PZ3**). TDDFT calculations demonstrated that the values of excitation energy from the S_0 state to the S_1 state are 2.86 eV for **PZ1**, 2.87 eV for **PZ2**, and 2.73 eV for **PZ3** (Fig. 5 and Table S6, ESI†). Moreover, the DFT calculations revealed that the highest occupied molecular orbital (HOMO) and the lowest unoccupied molecular orbital (LUMO) energy levels of **PZ3** are lower than those of **PZ1**, but the lowering in the LUMO energy level is larger than that in the HOMO energy level (Fig. S15, ESI,† HOMO = −5.78 eV, LUMO = −2.64 eV for **PZ1** and HOMO = −6.00 eV, LUMO = −2.94 eV for **PZ3**). Thus, the bathochromic shift of the photoabsorption bands from **PZ1** to **PZ3** is mainly attributed to the stabilization of the LUMO energy level through the introduction of the electron-withdrawing 4-chlorobenzoyl group into the phenazinone skeleton, resulting in a decrease in the HOMO–LUMO band gap (ΔE_{H-L} = 3.14 eV and 3.06 eV for **PZ1** and **PZ3**, respectively). Consequently, the bathochromic shift of the calculated photoabsorption bands from **PZ1** to **PZ3** was in good agreement with the experimental results (Fig. 3a and Table 1). In addition, **PZ2** with a methoxymethoxy group also exhibited a photoabsorption band in a longer wavelength region by 9 nm, compared to **PZ1**. However, the DFT and TDDFT calculations showed almost the same values of ΔE_{H-L} (3.14 eV for **PZ1** and 3.16 eV for **PZ2**) and excitation energy (2.86 eV for **PZ1** and 2.87 eV for **PZ2**) between **PZ1** and **PZ2**, in which the HOMO and the LUMO energy levels of **PZ2** (HOMO = −5.72 eV and LUMO = −2.56 eV) are slightly higher than those of **PZ1** (HOMO = −5.78 eV and LUMO = −2.64 eV). Meanwhile, the bathochromic shift of the photoabsorption bands from **PZ1** to **PZ2** would be explained based on the extended Hammett equation.[18] Thus, it is suggested that the substitution of a methoxymethoxy group for a hydroxy group reduces the electron-donating effect on the phenazinone chromophore because the substituent constants of hydroxy and methoxy groups are −0.37 and −0.268, respectively, leading to the bathochromic shift of the photoabsorption bands from **PZ1** to **PZ2**. In the corresponding fluorescence spectra, **PZ** showed two fluorescence bands with a fluorescence maximum wavelength (λ_{max}^{fl}) at 440 nm and 555 nm, which would originate from the phenazine skeleton and its phenoxide ion, respectively. On the other hand, **PZ1**, **PZ2**, and **PZ3** showed a fluorescence band with a λ_{max}^{fl} of 554 nm, 579 nm, and 597 nm, respectively, originating from phenazinone skeleton. The fluorescence quantum yields (Φ_{fl}) of **PZ1**, **PZ2**, and **PZ3** were significantly low (0.03 for **PZ1**, 0.04 for **PZ2**, and 0.05 for **PZ3**), which is attributed to ISC and IC as discussed later.

$^1O_2$ generation

Thus, we evaluated the $^1O_2$ generation ability of the phenazinone PSs **PZ1–3**. It is well-known that 1,3-diphenylisobenzofuran (DPBF) acts as an efficient $^1O_2$ scavenger to produce its oxidized product, *o*-dibenzoylbenzene.[19] Thus, $^1O_2$ generation by **PZ1–3** in THF was investigated by monitoring the photoabsorption spectral changes of DPBF accompanied by the reaction of DPBF with the generated $^1O_2$ (Fig. 4a–c). THF was bubbled with air for 10 min prior to preparing solutions. Air-saturated THF solutions containing DPBF and each PS were irradiated with monochromatic light at 509 nm (300 μW cm^{-2}) that was obtained by passage of a xenon light source through a monochromator. In all the solutions, the photoabsorption of DPBF at around 413 nm decreased with photoirradiation time, which indicates that DPBF reacted with $^1O_2$ generated by the photoexcitation of the PSs. However, the decrements in absorbance at 413 nm were significantly different between the PSs. Thus, the changes in optical density (ΔOD) of DPBF at 413 nm were plotted against photoirradiation time to estimate Φ_Δ values of these PSs (Fig. 4d): the Φ_Δ values were estimated from the slopes (m_{sam}) of the plots using rose bengal (RB, Φ_Δ = 0.68 in THF) as a standard sample (Table 1). The correlation coefficient (R^2) values for the calibration curves of **PZ1–3** and RB were 0.992–0.999, which indicates good linearity, and the m_{sam} values increased in the order of **PZ3** (0.0010) < **PZ2** (0.0070) < RB (0.0083) < **PZ1** (0.010). As the result, the Φ_Δ values were estimated to be 0.54, and 0.069 for **PZ2** and **PZ3**, respectively. It is worth noting here that **PZ1** exhibited the

Table 1 Optical data and $^1O_2$ quantum yields (Φ_Δ) of **PZ** and **PZ1–3** in THF

Dye	λ_{max}^{abs} (nm), (ε (M^{-1} cm^{-1}))	λ_{max}^{fl} (nm), (Φ_{fl}[a])	τ_{fl}[b] (ns)	Φ_Δ[c]
PZ	390 (17 500), 480 (1700)	440, 555 (<0.02), 558 (0.09)	2.13, 3.54,[d] 2.89[e]	0.28
PZ1	378 (15 700), 478 (10 900)	554 (0.03)	3.40[e]	0.86
PZ2	361 (10 500), 487 (8300)	579 (0.04)	3.26[e]	0.54
PZ3	349 (7700), 510 (8100)	597 (0.05)	1.14[e]	0.069

[a] Fluorescence quantum yields (λ_{ex} = λ_{max}^{abs}) were determined by using a calibrated integrating sphere system. [b] Fluorescence lifetimes. [c] $^1O_2$ quantum yields (relative decomposition rate of DPBF (1,3-diphenylisobenzofuran)) using RB as a standard (Φ_Δ = 0.68 in THF) and DPBF as a $^1O_2$ scavenger. The Φ_Δ values were estimated under assumption that the reactivity of $^1O_2$ was independent of the kind of solvents. [d] Photoexcited at 366 nm. [e] Photoexcited at 451 nm.

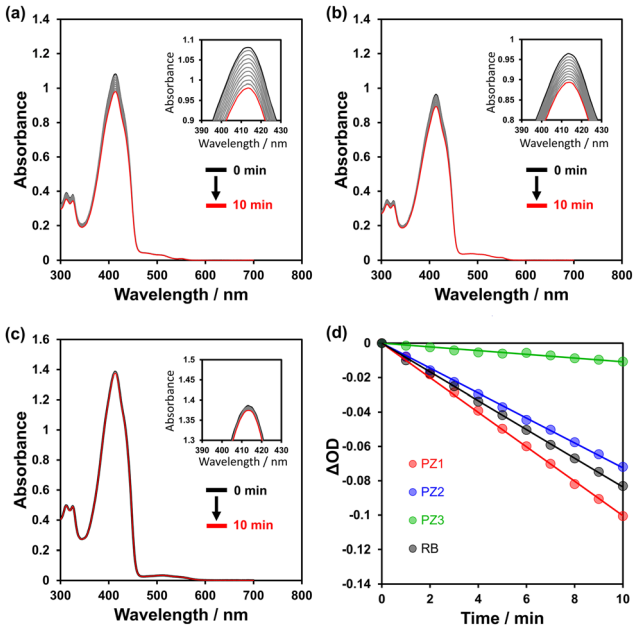

Fig. 4 Photoabsorption spectra of DPBF (5×10^{-5} M) in the presence of (a) **PZ1**, (b) **PZ2**, and (c) **PZ3** (abs.@509 nm = *ca.* 0.03) upon irradiation with monochromatic light (509 nm, 300 μW cm^{-2}) in THF. Insets are magnifications of peak tops in the spectra around 410 nm. (d) Plots of ΔOD of DPBF at 413 nm against photoirradiation time (509 nm, 300 μW cm^{-2}) in the presence of **PZ1**, **PZ2**, **PZ3**, and RB.

highest $^1O_2$ generation ability (Φ_Δ = 0.86). Indeed, the Φ_Δ values of **PZ1** and **PZ2** are higher than those of **KO-0–3** as well as **PZ** (Φ_Δ = 0.036–0.41 for **KO-0–3** and 0.33 for **PZ**). Thus, it was found that the phenazinone-based PS **PZ1** without halogen atoms possesses the superior $^1O_2$ generation ability to RB (Φ_Δ = 0.68 in THF) with many halogen atoms as well as MB (Φ_Δ = 0.57 in dichloromethane)[21] without halogen atoms.

Photophysical processes

In order to clarify the optical factors affecting the Φ_Δ values, we investigated the photophysical processes of the phenazinone-based PSs **PZ1–3** for $^1O_2$ generation. In this context, the radiative (k_r) and nonradiative (k_{nr}) decay rate constants were evaluated from the Φ_{fl} and fluorescence lifetime (τ_{fl}) values (Table 1) according to eqn (1) and (2):[22]

$$k_r = \Phi_{fl}/\tau_{fl} \quad (1)$$

$$k_{nr} = (1 - \Phi_{fl})/\tau_{fl} \quad (2)$$

In addition, the ISC (k_{ISC}) and IC (k_{IC}) rate constants were also evaluated according to eqn (3) and (4):

$$k_{ISC} = \Phi_T/\tau_{fl} \quad (3)$$

$$k_{nr} = k_{IC} + k_{ISC} \quad (4)$$

where the triplet generation quantum yield (Φ_T) was approximated by Φ_Δ.[23] Table 2 summarizes the values of k_r, k_{nr}, k_{ISC}, and k_{IC} for **PZ1–3**. The k_r values of all these PSs were low ($0.86–2.5 \times 10^7$ s^{-1}) due to the low Φ_{fl} values (≤ 0.05). **PZ3** showed a significantly low k_{ISC} value relative to the k_{nr} value,

Table 2 Rate constants in photophysical processes for **PZ1–3**

Dye	k_r ($\times 10^7$ s^{-1})	k_{nr} ($\times 10^7$ s^{-1})	k_{ISC} ($\times 10^7$ s^{-1})	k_{IC} ($\times 10^7$ s^{-1})
PZ1	1.3	28.1	25.4	2.8
PZ2	0.86	29.8	16.7	13.1
PZ3	2.5	85.3	6.1	79.2

resulting in a high k_{IC}/k_{nr} value (= 0.93). This high k_{IC}/k_{nr} value is ascribable to the vibrational relaxation to the lowest excited state caused by a flexible 4-chlorobenzoate group. On the other hand, **PZ1** without a flexible substituent showed a significantly low k_{IC}/k_{nr} value (= 0.10), and thus the k_{ISC} value accounts for much of the k_{nr} value. **PZ2** showed a relatively small k_{IC}/k_{nr} value (= 0.44) due to the methoxymethoxy group with moderate flexibility, resulting in the moderate k_{ISC}.[24] Consequently, these evaluations suggested that Φ_Δ values of **PZ1–3** depend on k_{ISC}, and thus **PZ1** with high k_{ISC} shows a high Φ_Δ value.

Theoretical calculations

To further understand the photophysical processes, DFT and TDDFT calculations were performed for **PZ** and **PZ1–3** at the B3LYP/6-311G(d,p) level,[26] in which the methoxymethyl group of **PZ2** was replaced with the methyl group for convenience of calculation. The optimized structures of **PZ1–3** showed high planarity despite the presence of an sp^3 nitrogen atom (Tables S2–S5 and Fig. S11–S14, ESI†) and are in good agreement with those obtained from the X-ray single crystal analysis. In the TDDFT calculations, the vertical excitation energies from the S_0 state to the S_n and T_n states for **PZ** and **PZ1–3** were calculated using the S_0 state geometry (Fig. 5, Tables S6, S7, and Fig. S16, ESI†). The oscillator strengths (f) for the S_0 to the S_1 state of **PZ1–3** were higher than that of **PZ** (0.025 for **PZ**, 0.12 for **PZ1** and **PZ2**, and 0.19 for **PZ3**), indicating that the phenazinone PSs show stronger photoabsorption as observed in the photoabsorption spectra (Fig. 3a). The TDDFT calculations also showed that each singlet and triplet excited states consisted of several types of transitions (Tables S6 and S7, ESI†). Therefore, in order to simplify the process for characterizing transitions in each excited state, the NTO calculations[25] were performed based on TDDFT results. As shown in Fig. 5, the unoccupied and occupied NTOs are expressed as "particle" and "hole" transition orbitals, respectively. It was found that for **PZ1–3** the energy gaps (ΔE_{ST}) between the S_1 state and the T_3 state were similar to each other (ΔE_{ST} = 0.34, 0.33, and 0.20 eV for **PZ1**, **PZ2**, and **PZ3**, respectively, Fig. 5 and Table S9, ESI†), indicating that ISC transitions from the S_1 state to the T_3 state were thermodynamically feasible. In addition, the hole of the T_3 state for **PZ1–3** is localized on the carbonyl oxygen with the *n*-orbital character, and the others (*i.e.*, the particle of the S_1 and the T_3 state, and the hole of the S_1) are delocalized over the phenazinone skeleton with the π-orbital character. These results suggested that the S_1 states of the **PZ1–3** are $^1(\pi\pi^*)$, which would undergo the transition to the T_3 state characterized by $^3(n\pi^*)$ according to the El-Sayed rule.[15] Thus, the NTO calculations demonstrated that the n orbitals on the carbonyl oxygen in the **PZ1–3** play an essential role in facilitating ISC

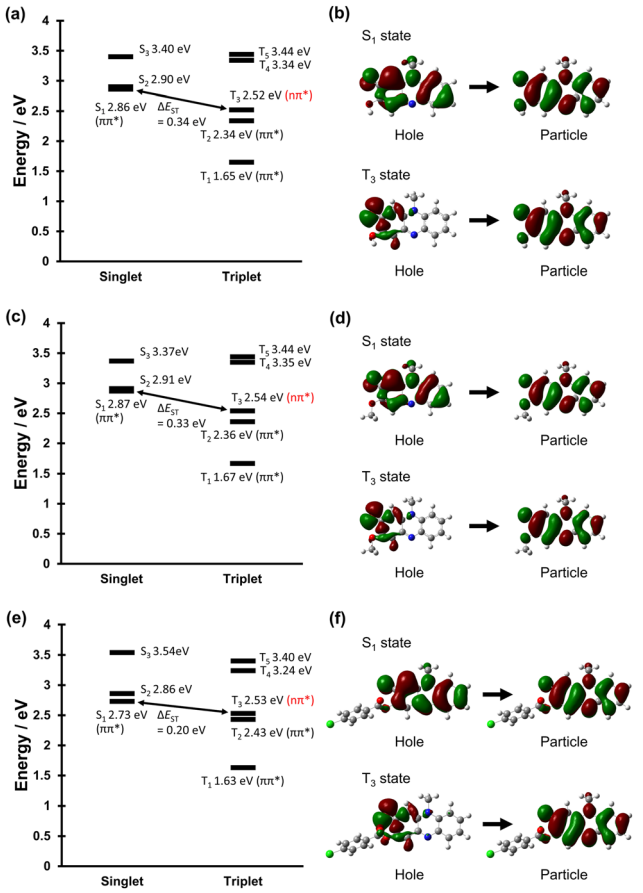

Fig. 5 Schematic diagrams showing vertical excitation energies of (a) **PZ1**, (c) **PZ2**, and (e) **PZ3** for three lowest singlet and five lowest triplet excited states, and natural transition orbital (NTO) images of S_1 and T_3 excited states of (b) **PZ1**, (d) **PZ2**, and (f) **PZ3**. The methoxymethyl group of **PZ2** was replaced with the methyl group for convenience of calculation.

from the S_1 to the T_3 state. Consequently, this work revealed that the phenazinone chromophores possess thermodynamically feasible ISC characteristics from the S_1 to the T_3 state (ΔE_{ST} = 0.20–0.36 eV) based on the El-Sayed rule, and thus the Φ_Δ values of **PZ1–3** are dominated by the k_{ISC}, which is decreased by the flexible substituent.

Conclusions

In conclusion, we have designed and developed the phenazinone derivatives **PZ1**, **PZ2**, and **PZ3** with a hydroxy, a methoxymethoxy, and a 4-chlorobenzoate substituent, respectively, as halogen-free-heteroanthracene-based PSs. It was found that the phenazinone incorporating a carbonyl group into the skeleton allows an efficient ISC based on the El-Sayed rule. Indeed, **PZ1** exhibited a high $^1O_2$ generation ability (Φ_Δ = 0.86), which is a superior photosensitizing ability to **PZ2** (Φ_Δ = 0.54) and **PZ3** (Φ_Δ = 0.069) with a flexible substituent. Consequently, we propose that the phenazinone skeleton is one of the promising halogen-atom-free-heteroanthracene-based chromophores as photosensitizers.

Experimental

General

All solvents and reagents were used as received unless otherwise noted. Rose bengal (RB) was purchased from Sigma Aldrich and recrystallized from methanol twice. 1,3-Diphenylisobenzofuran (DPBF) was purchased from Tokyo Chemical Industry and recrystallized from a mixture of dichloromethane and methanol.

^{1}H NMR and ^{13}C NMR spectra were recorded using Varian-400 (400 MHz) and Varian-500 (500 MHz) FT NMR spectrometers. FT-IR spectra were recorded using a Shimadzu IRTracer-100. High-resolution mass spectral data were acquired using a Thermo Fisher Scientific LTQ Orbitrap XL. Photoabsorption spectra were recorded using Shimadzu UV-3600-plus spectrophotometers. Fluorescence spectra were measured using a Hitachi F-4500 and HORIBA FluoroMax-4 spectrophotometer. The fluorescence quantum yields (Φ_{fl}) were determined using a Hamamatsu C9920-01 instrument equipped with CCD by using a calibrated integrating sphere system. Fluorescence decay measurements were performed using a HORIBA Delta-Flex modular fluorescence lifetime system, using a Nano LED pulsed diode excitation source (366 nm and 451 nm). The irradiance of monochromatic light (509 nm) for photosensitizing reactions was adjusted using a Newport 1918-C optical power meter.

Synthesis

3-Hydroxy-10-methylphenazin-2(10*H*)-one (PZ1). A solution of 2,5-dihydroxy-1,4-benzoquinone (0.145 g, 1.04 mmol) and *N*-methyl-*o*-phenylenediamine (0.127 g, 1.04 mmol) in ethanol (40 mL) was stirred at 80 °C. After the disappearance of the reactants, the reaction mixture was cooled to room temperature, and the precipitate was filtered and washed with a small amount of ethanol to give **PZ1** as a black solid (0.146 g, 62% yield); m.p. over 300 °C; IR (ATR): $\tilde{\nu}$ = 3179, 1587, 1572, 1545, 1501, 1468 cm^{-1}; ^{1}H NMR (400 MHz, DMSO-d_6, ppm): δ = 7.86–8.07 (m, 2H, aromatic), 7.72 (dd, J = 6.7 Hz, 1.5 Hz, 1H, aromatic), 7.51 (dd, J = 7.5 Hz, 0.5 Hz, 1H, aromatic), 6.86 (s, 1H, aromatic), 6.37 (s, 1H, aromatic), 3.94 (s, 3H, CH_3); ^{13}C NMR (125 MHz, DMSO-d_6, ppm): δ = 176.28, 156.64, 147.93, 136.55, 135.53, 130.60, 130.13, 129.45, 124.25, 115.21, 105.89, 97.04, 34.40; HRMS (APCI): m/z found 227.08127 $[M + H]^+$, calculated for $C_{13}H_{11}N_2O_2$ $[M + H]^+$: 227.08150.

3-Methoxymethoxy-10-methylphenazin-2(10*H*)-one (PZ2). A solution of sodium hydride abt. 60% oil suspension (80.6 mg) and **PZ1** (45.9 mg, 0.203 mmol) in DMF (30 mL) was stirred at 0 °C for 30 min. Then, chloromethyl methyl ether (150 μL, 1.98 mmol) was added to the solution, and the mixture was stirred at 0 °C overnight. The reaction was quenched with water, and then the solution was extracted with CH_2Cl_2. The organic layer was dried over anhydrous $MgSO_4$, filtered, and concentrated. The resulting residue was dissolved in CH_2Cl_2 and subjected to reprecipitation by hexane to afford **PZ2** as a reddish brown solid (35.5 mg, 63.4% yield); m.p. 195–198 °C; IR (ATR): $\tilde{\nu}$ = 2967, 2918, 2828, 1630, 1591, 1572, 1545, 1508 cm^{-1}; ^{1}H NMR (500 MHz, acetone-d_6, ppm): δ = 7.92 (dd, J = 8.1 Hz,

1.5 Hz, 1H, aromatic), 7.86 (d, J = 8.7 Hz, 1H, aromatic), 7.70 (dd, J = 7.0 Hz, 1.5 Hz, 1H, aromatic), 7.46 (dd, J = 7.0 Hz, 1.2 Hz, 1H, aromatic), 7.03 (s, 1H, aromatic), 6.17 (s, 1H, aromatic), 5.39 (s, 2H, CH_2), 3.91 (s, 3H, CH_3), 3.50 (s, 3H, CH_3); ^{13}C NMR (125 MHz, acetone-d_6, ppm): δ = 177.56, 156.98, 149.54, 136.77, 131.91, 131.14, 124.61, 115.36, 110.68, 99.93, 95.55, 56.90, 34.35; HRMS (APCI): m/z found 271.10785 $[M + H]^+$, calculated for $C_{15}H_{15}N_2O_3$ $[M + H]^+$: 271.10772.

3-(*p*-Chlorobenzoyl)-10-methylphenazin-2(10*H*)-one (PZ3). A solution of sodium hydride abt. 60% oil suspension (39.5 mg) and **PZ1** (46.0 mg, 0.203 mmol) in DMF (30 mL) was stirred at 0 °C for 20 min. Then, 4-chlorobenzoyl chloride (128 μL, 1.00 mmol) was added to the solution, and the mixture was stirred at 0 °C overnight. The reaction was quenched with water, and then the solution was extracted with CH_2Cl_2. The organic layer was dried over anhydrous $MgSO_4$, filtered, and concentrated. The crude was dissolved in toluene, and GPC was performed to give **PZ3** as a red solid (47 mg, 63% yield); m.p. 233–236 °C; IR (ATR): $\tilde{\nu}$ = 3067, 3044, 2924, 2853, 1923 cm^{-1}; ^{1}H NMR (400 MHz, DMSO-d_6, ppm): δ = 8.08–8.17 (m, 2H, aromatic), 7.99–8.08 (m, 2H, aromatic), 7.84 (t, J = 7.8 Hz, 8.0 Hz, 1H, aromatic), 7.67–7.77 (m, 3H, aromatic), 7.56 (t, J = 7.8 Hz, 7.6 Hz, 1H, aromatic), 6.40 (s, 1H, aromatic), 3.93 (s, 3H, CH_3); ^{13}C NMR (100 MHz, acetone-d_6, ppm): δ = 174.04, 162.62, 151.75, 146.16, 139.08, 137.52, 135.29, 132.85, 131.70, 131.43, 130.39, 129.13, 127.28, 124.38, 121.82, 115.27, 98.81, 34.43; HRMS (ESI): m/z found 365.06900 $[M + H]^+$, calculated for $C_{20}H_{14}N_2O_3Cl$ $[M + H]^+$: 365.06875.

X-Ray crystallographic analysis

The reflection data were collected at 100 K on a Bruker AXS SMART APEX II ULTRA diffractometer using monochromated Mo-Kα (λ = 0.71073 Å). The structure was solved by the SHELXT 2014/5 method and refined based on full-matrix least squares on F^2 using SHELXL-2017/1. The non-hydrogen atoms were refined anisotropically. Hydrogen atoms were fixed geometrically and not refined. Crystallographic data have been deposited in the S3 Cambridge Crystallographic Data Centre (CCDC 2194829 for **PZ1**, CCDC 2194831 for **PZ2**, and CCDC 2194832 for **PZ3**).†

Crystal of PZ1. A suitable crystal of **PZ1** was recrystallized from a mixed solvent of CH_2Cl_2/hexane as an air-stable, dark red block crystal. Crystallographic data: $C_{13}H_{10}N_2O_2$, M = 226.23, monoclinic, a = 6.7461(17), b = 6.8315(18), c = 21.892(6) Å, β = 93.503(3)°, V = 1007.0(4) Å^3, D_{calcd} = 1.492 g cm^{-3}, space group $P2(1)/n$ (no. 15), Z = 4, 4448 reflections measured, 2397 unique (R_{int} = 0.0477), which were used in all calculations. The final R_1(reflections) = 0.0434 (1714) $[I > 2\sigma(I)]$, wR_2(reflections) = 0.1197 (2397). GOF = 1.055 (Table S1, ESI†).

Crystal of PZ2. A suitable crystal of **PZ2** was recrystallized from a mixed solvent of CH_2Cl_2/hexane as an air-stable, dark red block crystal. Crystallographic data: $C_{15}H_{14}N_2O_3$, M = 270.28, monoclinic, a = 10.8605(18), b = 11.1311(18), c = 10.3566(17) Å, β = 96.649(2)°, V = 1243.6(4) Å^3, D_{calcd} = 1.444 g cm^{-3}, space group $P2(1)/c$ (no. 14), Z = 4, 6956 reflections measured, 2984 unique (R_{int} = 0.0335), which were used in all calculations. The final R_1(reflections) = 0.0389 (2449) $[I > 2\sigma(I)]$, wR_2(reflections) = 0.1037 (2984). GOF = 0.998 (Table S1, ESI†).

Crystal of PZ3. A suitable crystal of **PZ3** was recrystallized from a mixed solvent of CH_2Cl_2/hexane as an air-stable, red block crystal. Crystallographic data: $C_{20}H_{13}ClN_2O_3$, M = 364.77, monoclinic, a = 12.9125(8), b = 17.0395(10), c = 7.2712(4) Å, β = 93.9830(10)°, V = 1595.96(16) Å^3, D_{calcd} = 1.518 g cm^{-3}, space group $P2(1)/c$ (no. 14), Z = 4, 12 633 reflections measured, 3827 unique (R_{int} = 0.0202), which were used in all calculations. The final R_1(reflections) = 0.0340 (3316) $[I > 2\sigma(I)]$, wR_2(reflections) = 0.0818 (3827). GOF = 0.921 (Table S1, ESI†).

Evaluation of $^1O_2$ quantum yield

Quantum yields (Φ_Δ) for singlet oxygen ($^1O_2$) generation by **PZ1**, **PZ2**, and **PZ3** were evaluated by monitoring the changes in the photoabsorption spectra of 1,3-diphenylisobenzofuran (DPBF), a $^1O_2$ scavenger, in tetrahydrofuran (THF) upon photoirradiation. DPBF traps the generated $^1O_2$ to be oxidized. THF was bubbled with air for 10 min, prior to the preparation of the solutions. The concentration of DPBF was 5 × 10^{-5} M in the air-saturated THF solutions. The concentration of the photosensitizers (PSs) and rose bengal (RB) was adjusted so that the absorbance was *ca.* 0.03 at the irradiation wavelength (509 nm). The THF solutions containing DPBF and **PZ1**, **PZ2**, or **PZ3** were irradiated with monochromatic light (509 nm, 300 μW cm^{-2}) that was obtained by passage of a xenon light source (HAL-320, Asahi Spectra) through a monochromator (CMS-100, Asahi Spectra). Except for the nonirradiated solutions, each spectrum was measured immediately after photoirradiation for 1 min. The procedure was promptly repeated until the total photoirradiation time reached 10 min. The changes in optical density (ΔOD) of DPBF were plotted against photoirradiation time to obtain the slopes (m) and estimate Φ_Δ values. W. Wu *et al.* reported that RB shows a high $^1O_2$ generation with the Φ_Δ = 0.80 in MeOH.[20] To correct the difference of Φ_Δ values between MeOH and THF, the Φ_Δ values in THF were estimated from the following equation.

$$\Phi_{\Delta RB,THF} = \Phi_{\Delta RB,MeOH} \times [(m_{RB,THF}/m_{RB,MeOH}) \times (L_{RB,MeOH}/L_{RB,THF})]$$

where $m_{RB,MeOH}$ and $m_{RB,THF}$ are slopes in the plots of ΔOD at the photoabsorption maximum wavelength of DPBF (413 nm) against photoirradiation time, and $L_{RB,THF}$ and $L_{RB,MeOH}$ are light harvesting efficiencies, which are given by L = 1–10^{-A} ("A" is the absorbance at the photoirradiation wavelength). The $\Phi_{\Delta RB,THF}$ value was estimated to be 0.68 (Fig. S10, ESI†). The Φ_Δ values of **PZ1**, **PZ2**, and **PZ3** were determined by the relative method using RB (Φ_Δ = 0.68 in THF) as a standard according to the following equation:

$$\Phi_{\Delta sam} = \Phi_{\Delta ref} \times [(m_{sam}/m_{ref}) \times (L_{ref}/L_{sam})]$$

where $\Phi_{\Delta sam}$ and $\Phi_{\Delta ref}$ are $^1O_2$ quantum yields of phenazinone-based PSs and RB, respectively, m_{sam} and m_{ref} are slopes in the plots of ΔOD at the photoabsorption maximum wavelength of

DPBF (413 nm) against photoirradiation time, and L_{sam} and L_{ref} are light harvesting efficiencies, which are given by $L = 1–10^{-A}$ (''A'' is the absorbance at the photoirradiation wavelength).

Theoretical calculations

The Gaussian 16 program[26] was used for density functional theory (DFT) calculations, time-dependent DFT (TD-DFT) calculations, and natural transitional orbital (NTO) analysis. The S_0 geometries of **PZ** and **PZ1–3** were optimized *via* frequency calculations at the B3LYP/6-311G(d,p) level. There are no imaginary frequencies for all optimized structures. The TD-DFT calculations of both excited singlet and triplet states were performed using the optimized S_0 geometry at the B3LYP/6-311G(d,p) level. The methoxymethyl group of **PZ2** was replaced with the methyl group for convenience of calculations.

Conflicts of interest

There are no conflicts to declare.

Acknowledgements

This work was supported by a Grants-in-Aid for Scientific Research (B) from the Japan Society for the Promotion of Science (JSPS) KAKENHI Grant Number 22H02123 and by the Futaba Foundation.

Notes and references

1 D. G. Fresnadillo, *ChemPhotoChem*, 2018, **2**, 512–534.
2 K. A. Mariewskaya, A. P. Tyurin, A. A. Chistov, V. A. Korshun, V. A. Alferova and A. V. Ustinov, *Molecules*, 2021, **26**(13), 3971.
3 A. Kamkaew, S. H. Lim, H. B. Lee, L. V. Kiew, L. Y. Chung and K. Burgess, *Chem. Soc. Rev.*, 2013, **42**, 77–88.
4 M. C. Derosa and R. J. Crutchley, *Coord. Chem. Rev.*, 2002, **233–234**, 351–371.
5 B. Barut, C. Ö. Yalçın and Ü. Demirbaş, *J. Photochem. Photobiol., A*, 2021, **405**, 112946.
6 (*a*) K. Piwowar, A. Blacha-Grzechnik and J. Zak, *J. Electrochem. Soc.*, 2019, **166**, G163–G169; (*b*) F. Ronzani, A. Trivella, E. Arzoumanian, S. Blanc, M. Sarakha, C. Richard, E. Oliveros and S. Lacombe, *Photochem. Photobiol. Sci.*, 2013, **12**, 2160–2169.
7 T. M. Ebaston, F. Nakonechny, E. Talalai, G. Gellerman and L. Patsenker, *Dyes Pigm.*, 2021, **184**, 108854.
8 (*a*) L. Wang, J. Bai and Y. Qian, *New J. Chem.*, 2019, **43**, 16829–16834; (*b*) H. Wang, C. Li, Q. Wu, H. Wen, T. Sun and Z. Xie, *J. Mater. Chem. B*, 2022, **10**, 4967–4973; (*c*) M. Liu, C. Wang and Y. Qian, *New J. Chem.*, 2021, **45**, 18082–18089; (*d*) J. Chen, Y. Cui, K. Song, T. Liu, L. Zhou, B. Bao, R. Wang and L. Wang, *Biomater. Sci.*, 2021, **9**, 2115–2123; (*e*) I. J. Gomez, M. Russo, O. A. Arcidiacono, E. M. Sanchez-Carnerero, P. Klan and L. Zajickova, *Mater. Chem. Front.*, 2022, **6**, 1719–1726.
9 (*a*) Y. Ooyama, T. Enoki and J. Ohshita, *RSC Adv.*, 2016, **6**, 5428–5435; (*b*) A. Mohan, E. Sebastian, M. Gudem and M. Hariharan, *J. Phys. Chem. B*, 2020, **124**, 6867–6874.
10 O. J. Stacey and S. J. A. Pope, *RSC Adv.*, 2013, **3**, 25550–25564.
11 (*a*) J. Miao, Y. Huo, G. Yao, Y. Feng, J. Weng, W. Zhao and W. Guo, *Angew. Chem., Int. Ed.*, 2022, **61**, e202201815; (*b*) L. A. Ortiz-Rodriguez, S. J. Hoehn, A. Loredo, L. Wang, H. Xiao and C. E. Crespo-Hernández, *J. Am. Chem. Soc.*, 2021, **143**(7), 2676–2681.
12 R. W. Redmond and J. N. Gamlin, *Photochem. Photobiol.*, 1999, **70**, 391–475.
13 (*a*) Y. Hirata and I. Tanaka, *Chem. Phys. Lett.*, 1976, **43**, 568–570; (*b*) K. Imato, K. Ohira, M. Yamaguchi, T. Enoki and Y. Ooyama, *Mater. Chem. Front.*, 2020, **4**, 589–596.
14 K. Ohira, K. Imato and Y. Ooyama, *Meter. Chem. Front.*, 2021, **5**, 5298–5304.
15 (*a*) M. A. El-Sayed, *Acc. Chem. Res.*, 1968, **1**, 8; (*b*) M. Baba, *J. Phys. Chem. A*, 2011, **115**, 9514–9519; (*c*) S. Tsumura, K. Ohira, K. Hashimoto, K. Imato and Y. Ooyama, *Mater. Chem. Front.*, 2020, **4**, 2762–2771; (*d*) H. Shu, H. Li, J. Rao, L. Chen, X. Wang, X. Wu, H. Tian, H. Tong and L. Wang, *J. Mater. Chem. C*, 2020, **8**, 14360–14364.
16 M. Jäger, H. Görls, W. Günther and U. S. Schubert, *Chem. – Eur. J.*, 2013, **19**, 2150–2157.
17 K. Ogawa, M. Miura, T. Nakayama and J. Harada, *Chem. Lett.*, 2003, **32**(9), 840–841.
18 D. H. Mcdaniel and H. C. Brown, *J. Org. Chem.*, 1958, **23**(3), 420–427.
19 J. Zou, Z. Yin, P. Wang, D. Chen, J. Shao, Q. Zhang, L. Sun, W. Huang and X. Dong, *Chem. Sci.*, 2018, **9**, 2188–2194.
20 W. Wu, J. Sun, X. Cui and J. Zhao, *J. Mater. Chem. C*, 2013, **1**, 4577–4589.
21 L. Huang, X. Cui, B. Therrien and J. Zhao, *Chem. – Eur. J.*, 2013, **19**, 17472–17482.
22 Y. Hayashi, A. Morimoto, T. Maeda, T. Enoki, Y. Ooyama, Y. Matsui, H. Ikeda and S. Yagi, *New J. Chem.*, 2021, **45**, 2264–2275.
23 (*a*) S. Cekli, R. W. Winkel, E. Alarousu, O. F. Mohammed and K. S. Schanze, *Chem. Sci.*, 2016, **7**, 3621–3631; (*b*) R. D. Pensack, Y. Song, T. M. McCormick, A. A. Jahnke, J. Hollinger, D. S. Seferos and G. D. Scholes, *J. Phys. Chem. B*, 2014, **118**, 2589–2597.
24 P. F. Heelis, *Chem. Soc. Rev.*, 1982, **11**, 15–39.
25 (*a*) R. L. Martin, *J. Chem. Phys.*, 2003, **118**, 4775–4777; (*b*) C. Zhou, S. Zhang, Y. Gao, H. Liu, T. Shan, X. Liang, B. Yang and Y. Ma, *Adv. Funct. Mater.*, 2018, **28**, 1802407.
26 M. J. Frisch, G. W. Trucks, H. B. Schlegel, G. E. Scuseria, M. A. Robb, J. R. Cheeseman, G. Scalmani, V. Barone, G. A. Petersson, H. Nakatsuji, X. Li, M. Caricato, A. V. Marenich, J. Bloino, B. G. Janesko, R. Gomperts, B. Mennucci, H. P. Hratchian, J. V. Ortiz, A. F. Izmaylov, J. L. Sonnenberg, D. Williams-Young, F. Ding, F. Lipparini, F. Egidi, J. Goings, B. Peng, A. Petrone, T. Henderson, D. Ranasinghe, V. G. Zakrzewski, J. Gao, N. Rega, G. Zheng, W. Liang, M. Hada, M. Ehara, K. Toyota,

R. Fukuda, J. Hasegawa, M. Ishida, T. Nakajima, Y. Honda, O. Kitao, H. Nakai, T. Vreven, K. Throssell, J. A. Montgomery, Jr., J. E. Peralta, F. Ogliaro, M. J. Bearpark, J. J. Heyd, E. N. Brothers, K. N. Kudin, V. N. Staroverov, T. A. Keith, R. Kobayashi, J. Normand, K. Raghavachari, A. P. Rendell, J. C. Burant, S. S. Iyengar, J. Tomasi, M. Cossi, J. M. Millam, M. Klene, C. Adamo, R. Cammi, J. W. Ochterski, R. L. Martin, K. Morokuma, O. Farkas, J. B. Foresman and D. J. Fox, *Gaussian 16, Revision B.01*, Gaussian, Inc., Wallingford CT, 2016.

